CERN-SUMMER STUDENT REPORT

eleonora.pariset@cern.ch

$K^+ \to \pi^+\pi^0 a$ Analysis at the NA62 Experiment

Eleonora Pariset

Abstract

In this project, the analysis of the $K^+ \to \pi^+\pi^0 a$ decay, where a is a pseudoscalar particle with mass $m_a \in (0, 210)$ MeV going to invisible, is conducted. The analysis is based on data collected during the 2017B run of the NA62 experiment at CERN and builds upon previous preliminary investigations. Direct emission and interference backgrounds are included and evaluated as part of this study.

Supervisors:

Prof. Mauro Raggi
Prof.ssa Francesca Bucci
Dott.ssa Ilaria Panichi

Geneva, Switzerland
October 8, 2024

Contents

1 Introduction

This project focuses on developing an analysis framework to estimate the sensitivity of the NA62 experiment to the decay $K^+ \to \pi^+\pi^0 a$. A preliminary sensitivity study [1] was previously conducted for NA62 using a new Monte Carlo (MC) event generator based on the full differential decay rate of this channel. The objective of this project is to establish the analysis from the ground up, while integrating and expanding upon the earlier work.
The analysis workflow is structured into three steps:

1. applying the L0 hardware trigger;
2. implementing a preselection to filter out events inconsistent with the $K^+ \to \pi^+\pi^0 a$ signal and $K^+ \to \pi^+\pi^-$ (normalization) channels;
3. and performing the final signal and normalization selections.

This analysis uses data collected during the 2017B run period, with details of the MC samples used provided in Section 4.2.

2 Theoretical Motivation and State of the Art

This search aims to be as model-independent as possible, focusing on estimating the sensitivity to the decay $K^+ \to \pi^+\pi^0 a$, where a is a pseudoscalar particle interacting derivatively, with a mass in the range $m_a \in (0, 210)$ MeV/c^2. The theoretical motivations for this search are based on axion-like particle (ALP) models and, specifically, on the QCD axion in the case of a vanishing mass $m_a = 0$ MeV [2].

Axion-like particles are hypothetical pseudoscalar particles that could indicate new physics beyond the Standard Model (BSM). The decay $K^+ \to \pi^+\pi^0 a$ is of particular interest because it provides a way to test the axial-vector current couplings of pseudoscalars to quarks. In Quantum Chromodynamics (QCD), parity conservation ensures that only the axial-vector current contributes to this decay, distinguishing it from simpler decays like $K^+ \to \pi^+ a$, which probe the vector current [3]. Unlike QCD axions, in ALP models the mass m_a and decay constant f_a are free parameters, with the mass not necessarily determined by QCD dynamics but by other mechanisms, resulting in a looser constraint of $m_{\mathrm{ALP}} < 1$ GeV/c^2.

For QCD axions, the mass and coupling are fixed by QCD dynamics: $m_a \sim m_\pi \frac{f_\pi}{f_a}$ and $f_a^{-1} \sim g_{a\gamma\gamma}$. QCD axions arise from Peccei-Quinn (PQ) symmetry, which can mediate flavor-changing neutral currents (FCNCs) at the tree level. The axion was originally proposed to solve the *strong CP problem*, a fundamental issue in QCD that questions why CP symmetry is not strongly violated in strong interactions. This problem stems from the Chern-Simons term in the QCD Lagrangian:

$$L_{\theta\mathrm{QCD}} = \theta_{\mathrm{QCD}}\mathrm{Tr}\left(\frac{g^2}{32\pi^2}G_{\mu\nu}\tilde{G}^{\mu\nu}\right), \quad (1)$$

where $G_{\mu\nu}$ is the gluon field strength tensor and $\tilde{G}^{\mu\nu}$ is its dual. This CP-odd term should, in principle, generate CP-violating effects such as a neutron electric dipole moment (EDM). However, experimental constraints on the neutron EDM, currently limited to $|d_n| < 3.0 \times 10^{-26} e\,\mathrm{cm}$ [4], imply that the QCD vacuum angle θ_{QCD} must be extremely small ($\theta \leq 10^{-10}$), a value that the Standard Model does not naturally explain.

To address the strong CP problem, three primary solutions have been proposed: unconventional dynamics, spontaneous CP violation, and the Peccei-Quinn mechanism [5]. The Peccei-Quinn solution introduces a global chiral symmetry, $U(1)_{\mathrm{PQ}}$, which, when spontaneously broken, predicts the existence of a light pseudoscalar particle—the *axion*. This axion dynamically relaxes θ_{QCD} to zero, thereby solving the strong CP problem. In this framework, the axion is the Nambu-Goldstone boson of the PQ symmetry, and its mass and coupling are intrinsically tied to QCD dynamics.

This theoretical framework opens the door to the detection of axions or ALPs in decays such as $K^+ \to \pi^+\pi^0 a$, offering a unique opportunity to explore BSM physics.

An initial upper limit of approximately $BR < 10^{-5}$ at 90% confidence level was set by the ISTRA+ collaboration [6] in their search for a pseudoscalar sgoldstino. More recently, experimental results from the OKA collaboration [7] have improved the upper limits on the branching ratio for $K^+ \to \pi^+\pi^0 a$ for ALP masses between 0 and 200 MeV/c^2. These 90% confidence level upper limits range from 2.5×10^{-6} to 2.0×10^{-7}, except near the π^0 mass, where the limit is 4.4×10^{-6}.
The NA62 experiment, with its high-intensity kaon beam, has been identified as having the potential to investigate this decay [2].

3 The NA62 experiment at CERN

The NA62 experiment is fixed-target experiment at CERN situated in the North Area, whose primary analysis focuses on the rare decay $K^+ \to \pi^+\nu\bar{\nu}$. The layout of the NA62 beamline and detector is shown schematically in Fig.1 [8], along with the scale and reference system for the experimental layout.

An unseparated secondary beam of π^+ (70%), protons (23%) and K^+ (6%) is created by directing 400 GeV/c protons extracted from the CERN SPS onto a beryllium target in spills of 3s effective duration. The central beam momentum is 75 GeV/c, with a momentum spread of 1% (rms). The high momentum of the kaons in the laboratory

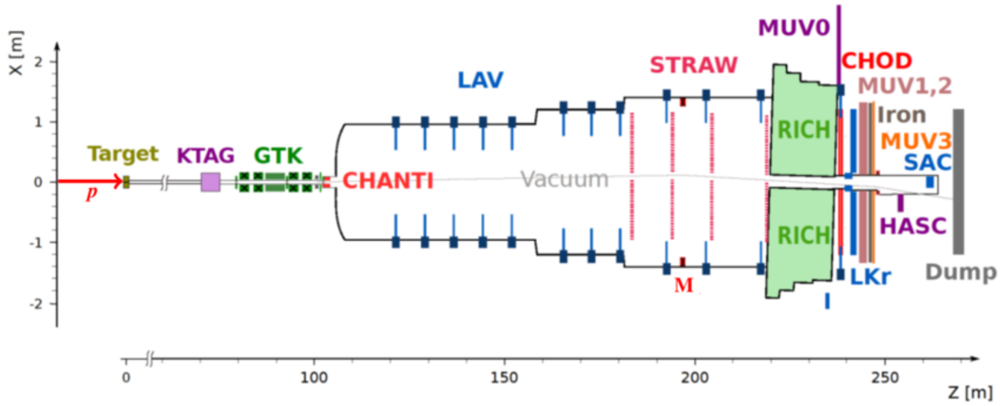

Figure 1: Schematic side view of the NA62 beamline and detector[8].

frame allows for precise measurements of the kinematic properties of the decay products. The rate is around 5 MHz of K^+ decays in the 65 m long decay region. The upstream detectors, that are exposed to a particle flux about 16 times larger than the kaon flux, measure the kaons' momentum and direction. Kaons are identified using a CEDAR differential Cherenkov counter equipped with a Kaon Tagger (KTAG). The incoming kaons' momentum and direction are measured using the GTK (GigaTracker), which consists of three stations with dipoles that provide excellent time and spatial resolution. A six-station plastic scintillator ring detector (CHANTI) vetoes against inelastic collisions occurring in the last station of the Gigatracker, that marks the beginning of the 65 m long fiducial decay region.
Downstream to the decay region, the trajectories and momenta of the charged decay products are measured using STRAW trackers, with two positioned before and two after a dipole magnet.
The downstream momentum spectrum is within $15 < p < 35$ GeV; outside this range, the Ring Imaging CHerenkov detector (RICH) detector's performance in particle identification deteriorates as $\beta \to 1$. The RICH is followed by a system of hodoscope counters (CHOD) to provide timing.
Decays involving photons (γ) in the final state are detected using a system of photon-veto detectors made up of a series of 12 Large Angle Vetoes (LAV), the Liquid Kripton (LKr) calorimeter, the Intermediate-Ring (IRC), and the Small Angle Calorimeter (SAC). For hadronic decays, two hadronic calorimeters (MUV01, MUV2) are used and a plane of scintillating tiles (MUV3) is employed as muon veto.

The comprehensive hermetic coverage of the NA62 experiment, necessary to achieve the primary physics objective of detecting the ultra-rare $K^+ \to \pi^+ \nu \bar{\nu}$ decay, also makes it ideally suited for investigating decays with missing energy and momentum, such as the one explored in this project.

3.1 Trigger

The intense flux of NA62 requires a high-performance trigger system. The beam intensity, defined in terms of the particle rate exiting the GTK, is 750 MHz, of which the 6% (i.e. 45 MHz) is K^+. The NA62 trigger system is arranged in two stages: a first low-level hardware trigger (L0) and a subsequent L1 software trigger stage. The data are collected through *trigger lines*, designed to select specific category of events. Different trigger streams accounts for different categories of potentially interesting events.

The *trigger line* used in this analysis is the *control line*. The *control line* collects minimum-bias events for calibration and data-quality monitoring.

The L0 trigger condition selects all events with in-time coincidences of the horizontal and vertical planes of the CHOD, ensuring that all events with at least one charged particle are selected. The selected events are then downscaled by a factor $D = 400$. Approximately 15% of the K mesons either do not decay or decay before entering the fiducial region. If the K meson decays within the fiducial region, there is at least one track detected by the CHOD.

3.2 Detectors

The detectors are divided into upstream and downstream detectors. The upstream detectors include the differential Cherenkov counter (KTAG) for K^+ identification, the silicon pixel beam tracker (GTK), and the anti-counter (CHANTI) designed to detect inelastic interactions between the beam and the GTK3. The downstream detectors consist of the track momentum spectrometer (STRAW), scintillator hodoscopes (CHOD), several calorimeters (LKr, MUV1, MUV2), a RICH Cherenkov counter for $\pi/\mu/e$ identification, photon veto detectors (LAV, SAV, IRC), and the muon detector (MUV3).

A short description of each detector is provided in the following paragraph.

- **Cedar/KTAG system**: K^+ mesons are identified using the CEDAR/KTAG system. This system is composed of a CEDAR module coupled with a specially designed photon detection and readout module, known as the KTAG detector. Together, they form a differential Cherenkov counter with achromatic ring focus.

  The CEDAR radiator volume is filled with 0.94 m^3 of N_2 gas at a pressure of 1.75 bar and room temperature. This setup is specifically chosen so that only Cherenkov light from K^+ mesons can pass through the KTAG's annular diaphragm, which has a fixed central radius and a variable radial aperture. The KTAG provides a time resolution of approximately 70 ps.
- **GigaTracker (GTK)**: The Gigatracker (GTK) is designed to track incoming beam particles, with the goal of precisely measuring the time, direction, and momentum of all beam tracks (approximately 10^9 per second). It consists of three stations, in vacuum, featuring silicon pixel detectors with dimensions of 300×300 μm and

a thickness of 200 μm, based on p-in-n technology. The GTK provides a time resolution of 200 ps per station (rms), an angular resolution of 14 mrad (rms), and a momentum resolution of 0.2%.

- **Charged Anti-Coincidence Counter (CHANTI)**: the Charged ANTI (CHANTI) detector is designed to reduce critical background caused by inelastic interactions of the beam with the collimator and the Gigatracker (GTK) stations, as well as to tag beam halo muons in the region immediately adjacent to the beam. The CHANTI system consists of six stations, with a hole in the middle for the beam to pass, positioned inside the vacuum tube at distances of 27 mm, 77 mm, 177 mm, 377 mm, and 777 mm from GTK-3. The CHANTI detector can veto approximately 95% of all inelastic interactions of kaons in GTK-3, regardless of the final state. This veto efficiency increases to nearly 99% when focusing on signal-like events—specifically, cases where the kaon either does not survive the inelastic interaction or does not decay within the fiducial volume, and a single track is reconstructed by the straw spectrometer. Each CHANTI station consists of two layers composed of scintillator bars oriented vertically and horizontally.
- **STRAW**: the Straw Tracker measures the direction and the momentum of secondary charged particles originating from the decay region. It operates in vacuum at 10^{-6} mbar and it is made up of 4 stations.
- **RICH**: the Ring Imaging CHerenkov (RICH) detector is designed for particle identification (PID), specifically to distinguish between π^+ and μ^+ of 15–35 GeV/c. It also allows to measure the pion crossing time with a resolution of approximately 100 ps. It is located between the last Straw Station (210 m from the target) and the last Large Angle Veto station. It consists of a cylindrical vessel approximately 18 m long with a decreasing diameter ranging from 3.2 m to 3.8 m, through which the beam pipe passes centrally. The vessel is filled with neon gas at 1 atm. At the downstream end, a mosaic of hexagonal mirrors focuses the Cherenkov light onto 2000 photodetectors positioned at the upstream end.
- **CHOD**: the system consists of 2 charged particle hodoscopes, the NA48-CHOD and the new NA62-CHOD, positioned between the RICH and LKr with active area covering radii between the IRC outer radius (145 mm) and LAV12 inner radius (1070 mm).
- **Muon Veto (MUV)**: it consists of three distinct parts, called MUV1, MUV2, and MUV3. MUV1 and MUV2 are positioned downstream of the LKr calorimeter and function as hadronic calorimeters, designed to measure the deposited energy and analyze the shower shapes of incident particles. These detectors are constructed as iron-scintillator sandwich calorimeters, with MUV1 consisting of 24 layers of scintillator strips and MUV2 comprising 22 layers. In both modules, the scintillator strips are arranged in alternating orientations—horizontal and vertical—across

successive layers to enhance spatial resolution and detection accuracy. MUV3 serves a dual purpose: it provides fast L0 trigger signals and is crucial for muon identification. This module is composed of two layers (x and y) of fast scintillators, placed immediately after an 80 cm thick iron wall. The design of MUV3 allows for efficient and rapid muon detection, ensuring timely data processing and trigger generation.

- **Liquid Krypton (LKr)**: the Liquid Krypton calorimeter (LKr) is a quasi-homogeneous electromagnetic calorimeter formed of a cryostat filled with 9000 litres of liquid krypton at 120 K. The LKr energy resolution is given by [8]:

$$\frac{\sigma_E}{E} = \frac{4.8\%}{\sqrt{E}} \oplus \frac{11\%}{E} \oplus 0.9\%.$$

  With a depth of 27 X_0, this calorimeter effectively contains the entire shower produced by photons and electrons ($e^{\pm}$). However, pions can initiate both electromagnetic and hadronic showers, which are less likely to be fully contained within the LKr. Muons, on the other hand, behave as minimum ionizing particles (MIPs), depositing only a small amount of energy as they pass through the detector. Due to these properties, the ratio E/p, where E is the energy deposited in the LKr and p is the momentum measured by the STRAW for a charged particle, can be utilized for particle identification. This ratio also plays a crucial role in the photon veto system.

- **Large-Angle Veto (LAV)**: the LAV system consists of 12 stations, with one positioned in air upstream of the LKr calorimeter and the remaining 11 placed along the vacuum volume of the decay region. These stations are designed to reject photons emitted at angles ranging from 8.5 to 50 mrad. Each station has a ring-shaped configuration, comprising 37 cm long lead-glass modules arranged radially. The Cherenkov light generated within each lead-glass block is captured by a 76 mm photomultiplier. To maximize radiation length, each station is built with multiple rings, providing a total minimum effective depth of 21 radiation lengths. The system achieves a time resolution of 1 ns for particles with 1 GeV energy and an energy resolution of better than 10%. This precision helps to maintain the accidental muon rate at approximately $\mathcal{O}(1\%)$. The photon vetoes are designed to ensure hermetic geometrical coverage up to 50 mrad for photons originating from kaon decays occurring within the decay region, specifically between 105 m and 170 m downstream of the target.

- **Small-Angle Veto (SAV)**: the small-angle veto system provides hermeticity for photons emitted at angles down to zero degrees with respect to the beam axis. It consists of two detectors: the intermediate-ring ralorimeter (IRC) and the small-angle calorimeter (SAC). Both are shashlyk calorimeters, with lead and plastic-scintillator plates traversed by wavelength-shifting (WLS) fibres. The IRC is situated before the LKr calorimeter and covers the region around the inner radius of the Liquid Krypton Calorimeter. The SAC is installed after the dipole magnet at the end of the beam pipe tha deflects the beam particles towards an off-axis beam dump. Neutral particles and photons that pass through the beam pipe can be detected by the SAC, which is aligned with the original beam axis.

4 Data Analysis

A cut-based analysis was implemented, based on the experimental signature of the decay, as described in Sec. 4.1. A first preselection stage (Sec. 4.3.2) was applied to reduce the data. After the preselection, the signal selection was performed (Sec. 4.3.3), along with a normalization procedure (Sec. 4.3.4).

4.1 Analysis strategy

The experimental signature of the decay consists of a single charged track, identified as a π^+, and two electromagnetic clusters in the LKr calorimeter that are not associated with any charged track. These clusters must be in-time with each other, as they originate from the decay $\pi^0 \to \gamma\gamma$, and in-time with the π^+.

Since the search is for an axion decaying into invisible there should be missing quadri-momentum $p_{miss} = (E_{miss}, \vec{p}_{miss})$.

$$\begin{cases} \vec{p}_{\rm miss} = \vec{p}_a = \vec{p}_K - \vec{p}_{\pi^+} - \vec{p}_{\pi^0} \\ E_{\rm miss} = E_a = E_K - E_{\pi^+} - E_{\pi^0} \end{cases} \tag{2}$$

Therefore, two interesting quantities to study the signal are the missing mass squared

$$m^2_{\rm miss} = m^2_a = (p_K - p_{\pi^+} - p_{\pi^0})^2 \tag{3}$$

and the square of the transverse component of the missing 3-momentum:

$$p_T^2 = |\vec{p}_{\rm miss} - \hat{p}_K(\vec{p}_{\rm miss} \cdot \hat{p}_K)|^2, \qquad \hat{p}_K = \frac{\vec{p}_K}{|\vec{p}_K|} \tag{4}$$

The main background sources are listed in Tab.1, along with the primary rejection tools. These Standard Model decays could mimic the signal's signature due to mismeasurement of the kinematics quantities and/or an undetected particles simulating an axion.

It is worth noting that in this analysis, the $K^+ \to \pi^+\pi^0\gamma$ internal Bremsstrahlung (IB), direct emission (DE), and interference (INT) contributions were all taken into account, unlike in the previous study [1]. The DE and INT contributions are indistinguishable from the signal under the mass hypothesis $m_a = 0$ MeV. The relative amounts of DE

Decay mode	BR	Main rejection tools
$K^+ \to \pi^+\pi^0(\gamma)$ (IB)	20.7%	$\gamma-$veto + kinematics
$K^+ \to \pi^+\pi^0\gamma$ (DE)	3.32% BR_{IB}	number of clusters
$K^+ \to \pi^+\pi^0\gamma$ (INT)	2.35% BR_{IB}	number of clusters
$K^+ \to \pi^+\pi^0\pi^0$ ($K_{3\pi^0}$)	1.76%	$\gamma-$veto + number of clusters
$K^+ \to \pi^+\pi^-\pi^+$ ($K_{3\pi}$)	5.58%	number of tracks
$K^+ \to \pi^0\mu^+\nu_\mu$ ($K_{\mu3}$)	3.35%	$\mu-$ID + $\gamma-$veto
$K^+ \to \pi^0 e^+\nu_e$ (K_{e3})	5.07%	$e-$ID + $\gamma-$veto
$K^+ \to \mu^+\nu_\mu(\gamma)$ ($K_{\mu2}$)	63.6%	$\mu-$ID + $\gamma-$veto

Table 1: Main background sources along with their branching ratios (BR) [9],[10] and main rejections tools.

and INT with respect to the IB contribution used in this analysis were measured in the range $0 < T^*_{\pi^+} < 80$ MeV [9]. Although small, these contributions must be accounted for; otherwise, they would result in a loss of sensitivity at $m_a = 0$ MeV.

4.2 Data and simulated samples

In this analysis the data sample recorded during 2017B run period, filtered with the *OnePionTwoClusters* filter (1P2C), was used. The MC samples used to study the backgrounds sources are listed in Tab.2.

Decay mode	NA62MC version	NA62Reconstruction version
$K^+ \to \pi^+\pi^0(\gamma)$ (IB)	3.8.5	3.8.5
$K^+ \to \pi^+\pi^0\gamma$ (DE)	3.2.7	3.7.6
$K^+ \to \pi^+\pi^0\gamma$ (INT)	3.2.7	3.7.6
$K^+ \to \pi^+\pi^0\pi^0$ ($K_{3\pi^0}$)	3.8.5	3.8.5
$K^+ \to \pi^+\pi^-\pi^+$ ($K_{3\pi}$)	3.9.0	3.9.0
$K^+ \to \pi^0\mu^+\nu_\mu$ ($K_{\mu3}$)	3.9.0	3.9.0
$K^+ \to \pi^0 e^+\nu_e$ (K_{e3})	3.9.0	3.9.0
$K^+ \to \mu^+\nu_\mu(\gamma)$ ($K_{\mu2}$)	3.9.0	3.9.4
signal with $m_a \in (0,210)$ MeV/c^2in steps of 10 MeV/c^2	3.8.9	3.8.9

Table 2: Monte Carlo (MC) samples versions and reconstruction version used for the analysis.

The MC samples play a fundamental role in the analysis, since they allow to study the effect of each cut on the various background sources. They were produced with the NA62MC versions and reconstructed with NA62Reconstruction versions specified in Tab.2. All MC samples were reconstructed in the *overlay* mode which is a technique that consists in adding hits from other MC events on top of the ones of the generated event. This allows to emulate accidental activity due to beam intensity.

To generate the MC signal sample the full differential rate, computed using lowest-order chiral perturbation theory [1], was used. In Fig.2a, 2b and 2c the phase space is shown for different mass hypothesis respectively $m_a = 0, 90, 150\ MeV$.

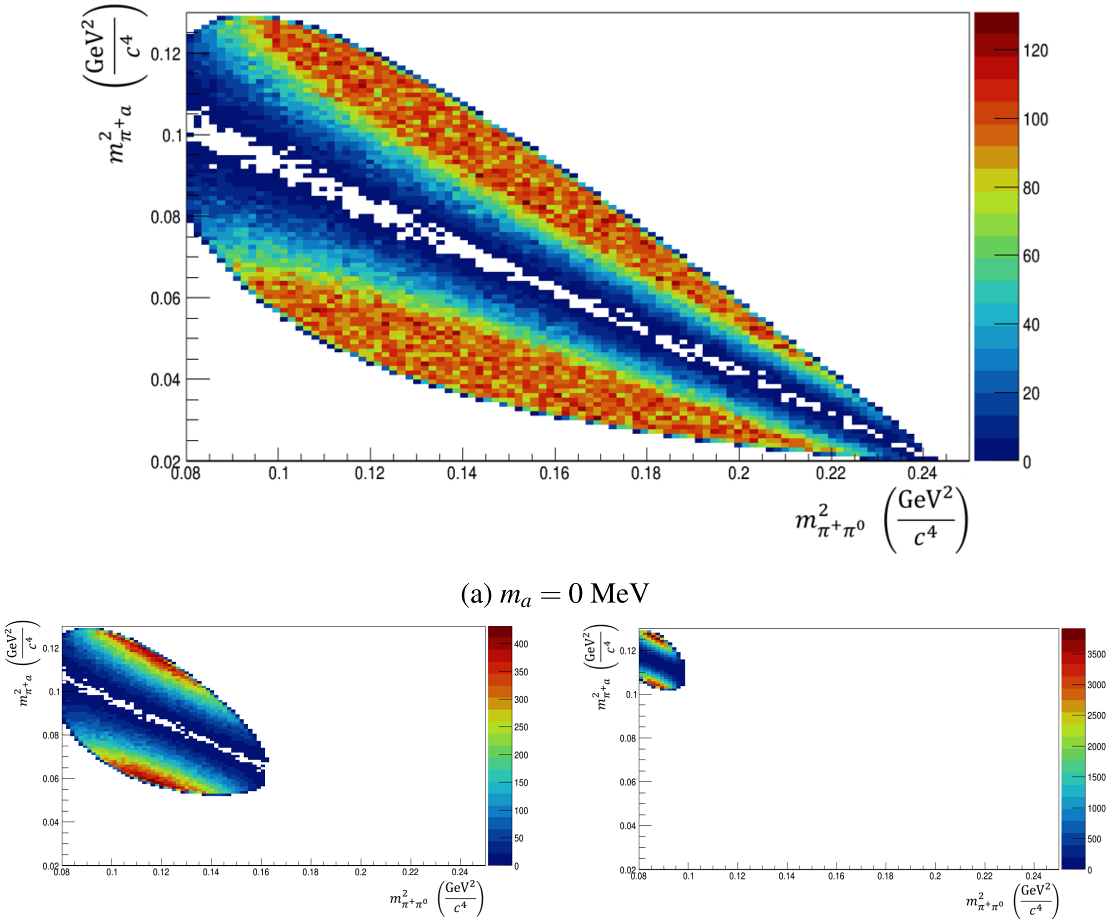

(a) $m_a = 0$ MeV

(b) $m_a = 90$ MeV

(c) $m_a = 150$ MeV

Figure 2: Dalitz plots of the $K^+ \to \pi^+\pi^0 a$ decay for MC samples at various mass hypotheses: $m_a = 0, 90, 150$ MeV.

4.3 Event Selection

The event selection process begins with a preselection stage, which applies common cuts for both the signal and normalization events. The dataset used was the 1P2C dataset, which was initially filtered using the `OnePionTwoClusters` filter (available in the framework na62fw/Analyzers/PhysicsTools/src/OnePionTwoClusters.cc). To ensure consistency, the same cuts from the 1P2C filter were reimplemented in the Preselection analyzer, either identically or with tighter criteria, allowing the selection to be applied to the MC samples as well. After the preselection stage, the analysis split into a signal selection, whose aim is selecting signal events, and a normalisation selection, necessary to compare the MC and data.

4.3.1 One Pion Two Clusters Filter

The data were filtered applying the 1P2C filter whose aim is to identify the *triplets*, defined as a positively charged downstream track and two clusters. It was therefore necessary to reimplement the cut of this filter, which basically consists in:

- The event passing the L0 Control trigger;
- A single positively charged track must be detected within the acceptance range of all four STRAWS stations;
- The fit of the STRAWS hits in the track reconstruction has $\chi^2 < 40$;
- The track time matches the trigger time within ± 20 ns;
- The decay vertex is within the fiducial decay region ($90 < z_{\text{vtx}} < 180$ m);
- The minimum distance between the track and the beam axis is less than 100 mm;
- The track's momentum, measured by STRAWS, is less than 70 GeV/c;
- For LKr clusters, the ratio $E/p < 0.95$;
- There are two in-time LKr energy clusters, each with energy > 3 GeV;
- The clusters and the track's impact points on the LKr must be more than 50 mm distant.

In addition, the events are flagged by the 1P2C filter as RARE or K2PI according to the following definitions.

- an event is flagged as **RARE** if:

$$m^2_{K^+-\pi^+} > 0.03\,\text{GeV}^2/c^4 \tag{5}$$

  thus looking for events with other particles than the π^0.

- an event is flagged as **K2PI** if:

$$65 < P_{\pi^+ + \pi^0} < 80\,\mathrm{GeV}/c$$
$$0.01 < m^2_{K^+ - \pi^+} < 0.03\,\mathrm{GeV}^2/c^4$$

  thus asking that the total final momentum is around the beam's momentum and the missing mass squared being the around the squared mass of the π^0. A downscaling $D_{K2PI} = 10$ is applied to these events.

Given the downscaling applied to K2PI-labeled events only(Fig. 3), it is crucial to use the same definitions of K2PI and RARE flags, as previously mentioned, in both the normalization and signal selection stages.

4.3.2 PRESELECTION

In the Preselection analyzer, I first reimplemented the cuts from the 1P2C filter (Sec.4.3.1), applying the same or stricter criteria while also excluding bad bursts. A strong cut requiring exactly 3 LKr calorimeter clusters and 1 downstream track is also applied. Such an aggressive cut should and will be relaxed in a more refined analysis.
Then, the idea is to first identify a good downstream track, recognized as π^+, and subsequently match it with a suitable upstream particle, determined to be a K^+, in order to locate the charged vertex. After that, the π^0 is identified selecting applying various cuts on the LKr clusters, leading to find the neutral vertex that must be close to the charged vertex. Finally the photon veto is applied. Let us now go over each step of the preselection process in detail.

- π^+ **identification**. First, some quality criteria are applied on the downstream track. The electric charge is required to be equal to $+1$, the `IsFake()` tracks are excluded. The track is required to be in the fiducial volume (105-180 m) and the detectors' acceptance and its momentum is required to be greater than 70 GeV/c. The reconstructed track must also have $\chi^2 < 20$, closest distance of approach CDA < 100. Of course the track is required to be in time with the trigger, whithin 20 ns. Only events with one downstream track are kept. Then, the particle identification is performed asking the track momentum to be in the range $(15, 45) GeV/c$ and requiring no in-time activity in MUV3 both spatially and temporally. In addition, the track must be identified ad π^+ by RICH thus requiring the RICH most likely hypothesis for the track to be a π^+ and asking for the maximum between the RICH likelihood hypothesis of positron, muon, kaon and background to be smaller than 0.5. A cut on $0.15 < E/p < 0.85$ is also applied, in addition to the one already present in the filter to exclude electrons. Given the charged downstream tracks, the ones associated with a cluster in the LKr calorimeter are excluded. A rematching of the cluster and time track is also performed requiring the time of the track and the cluster to be compatible within 3 ns.

- K^+ **identification**. Once identified the π^+, an upstream track in time with the selected downstream track is identified using the `SpectrometerGiga TrackerMatching()`, requiring the KTAG `GetNSectors` $\geq$ `5` and imposing the KTAG time to agree with the track time within 0.6 ns. A cut on the kaon momentum in range (72, 78) GeV/c is also applied. The charged vertex is also found.
- π^0 **identification**. First of all, the LKr clusters are filtered based on several conditions, such as being isolated (no neighboring significant energy hits) and at least 20 *mm* far from the nearest dead cells, being electromagnetic, being in the LKr calorimeter acceptance and having an energy greather than 3000 MeV. The clusters must not be associated with a spectrometer track. After this initial filtering, good pair of clusters are selected based on various time-based criteria. The time difference between the two clusters must not exceed a threshold set to be 3 ns. Both clusters have also to be synchronised, within 1.5 ns, with the track time. Additional calculations and checks are performed, such as calculating the spatial distance between clusters and the distance of each clusters from the the track with and without the magnet influence. The invariant mass of the photon pair (i.e. the π^0 candidate) is therefore computed and required to be in the range $(110, 160)$ MeV/c^2. The best pair is found minimizing the diphoton mass. After looping through all potential pairs, the code checks if exactly one good pair has been found. The neutral vertex is therefore found and events whose distance between the neutral and the charged vertex is greater than 7000 *mm* are excluded.
- **Photon veto**. The LAV matching is performed excluding events with associated LAV signals within 3 ns. The SAV and IRC matching exclude events with signals from these detectors within 7 ns.

The preselection analyzer gives as output the selected downstream track, the pair of good LKr clusters found along with the selected upstream track.

4.3.3 SIGNAL ANALYZER

On top of the preselection, the RARE flag is required and a tighter cut on the diphoton mass being in range $(125, 145)$ MeV is required. At this point of the signal selection, two interesting quantities to study the signal are m^2_{miss} and p^2_T, as explained in Sec.4.1. The 2D distributions of these variables are shown for the data, the various MC background sources and the MC signal respectively in Fig.4, 5 and 6. At this stage of the signal selection, the main background contributions from IB, DE, K3PI, K3PI0 are identifiable in the data.
As this signal search is based on the m^2_{miss} variable, the m^2_{miss} distribution is displayed

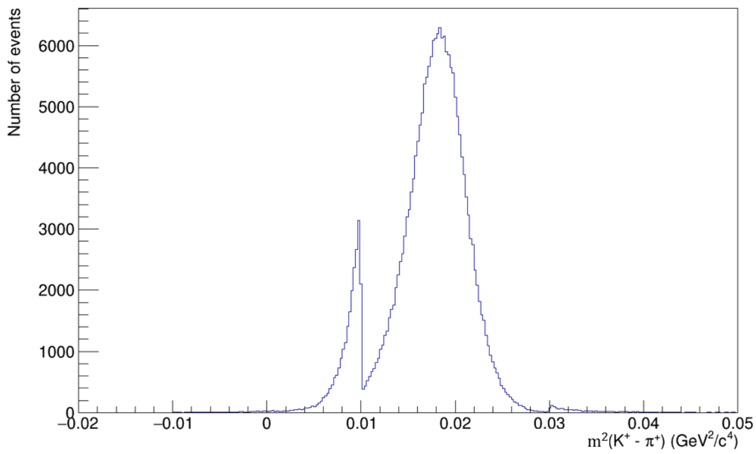

Figure 3: Plot of $m^2_{K^+-\pi^+}$ at the end of the preselection. The effect of the downscaling $D_{K2PI} = 10$ is evident.

in Fig. 7. The MC samples for the background channels are stacked, while the data sample is plotted separately. It is important to emphasize that, to make this plot, it is crucial to correctly account for the downscaling factor D_{K2PI} and properly normalize the MC samples (Sec.4.4). An additional step could involve exploring methods to further suppress the K3PI background.

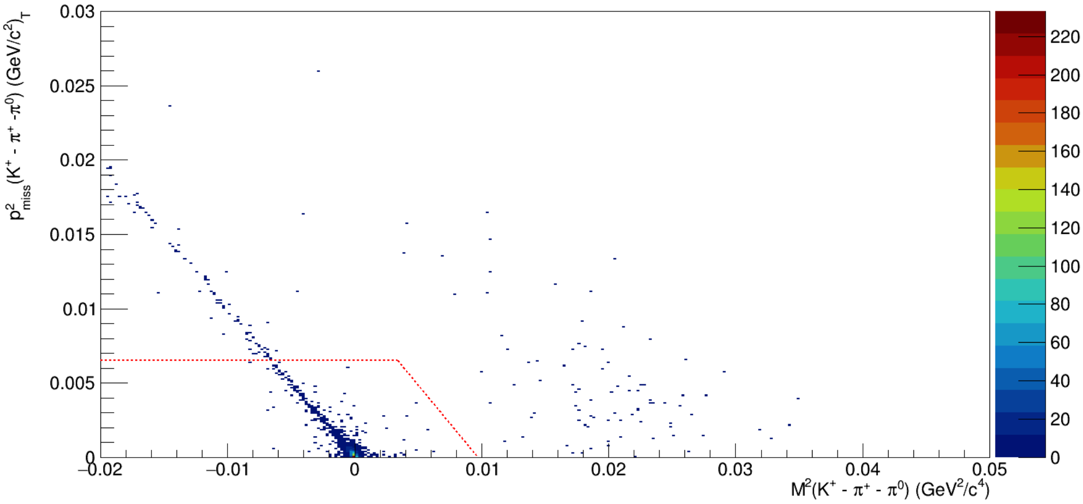

Figure 4: p_T^2 vs m^2_{miss} distribution for the data, after the signal selection cuts are applied. The trapezoidal cut is shown in red, meaning that the region below the dotted red line is rejected.

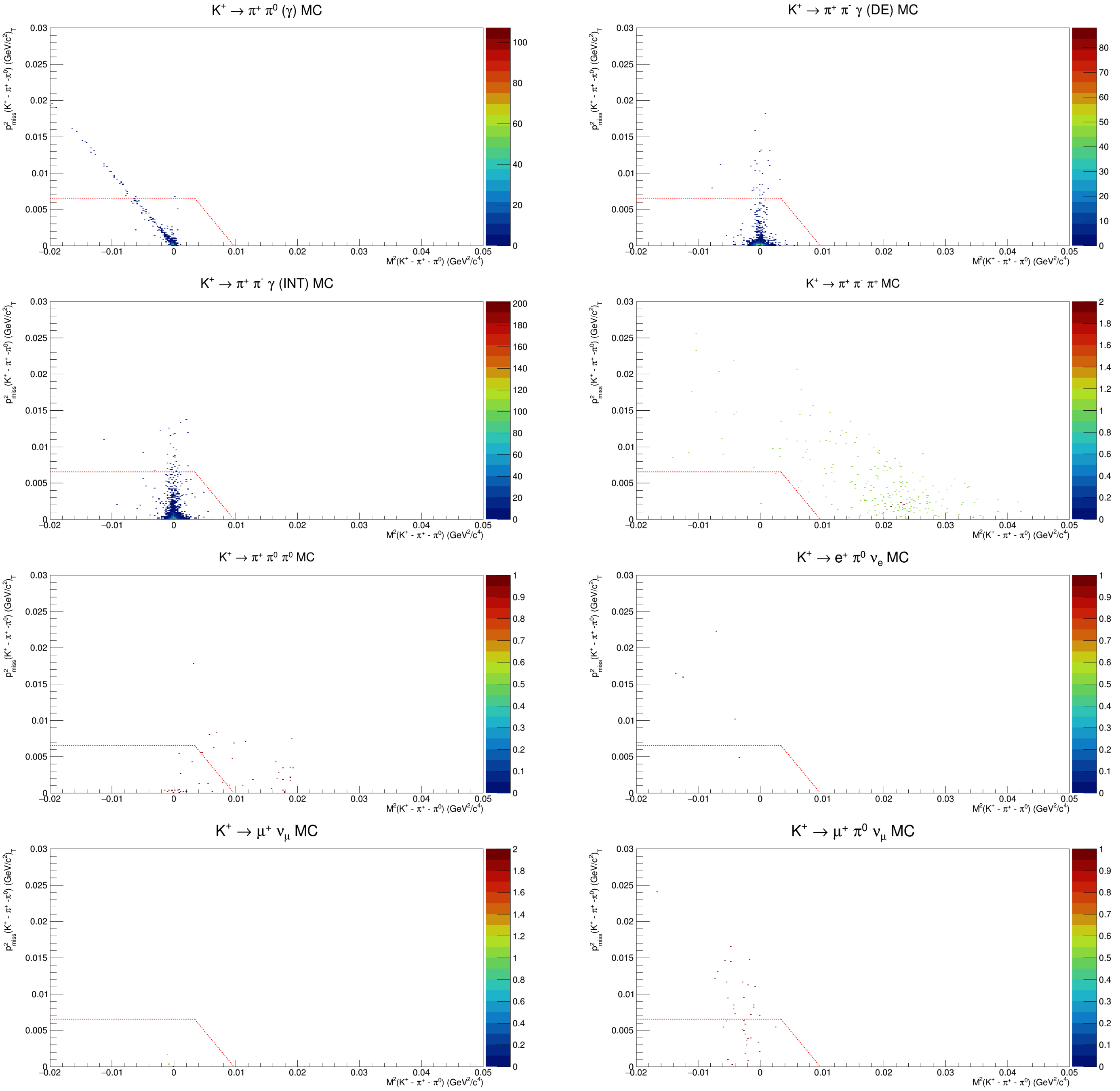

Figure 5: p_T^2 vs m_{miss}^2 distribution for the MC backgrounds, after the signal selection cuts are applied. The trapezoidal cut is shown in red, meaning that the region below the dotted red line is rejected.

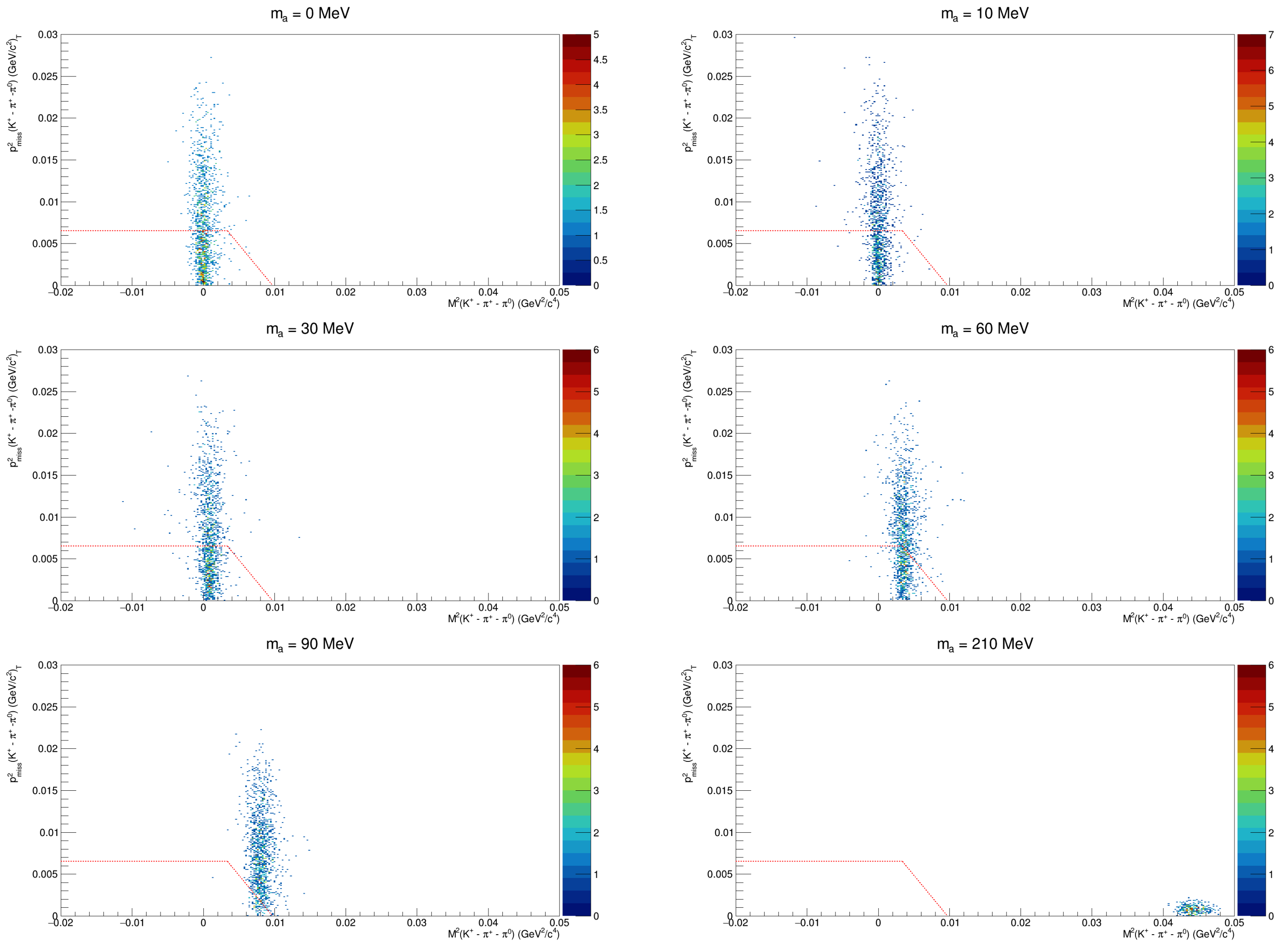

Figure 6: p_T^2 vs m_{miss}^2 distribution for various signal's mass hypotheses, after the signal selection cuts are applied. The trapezoidal cut is shown in red, meaning that the region below the dotted red line is rejected.

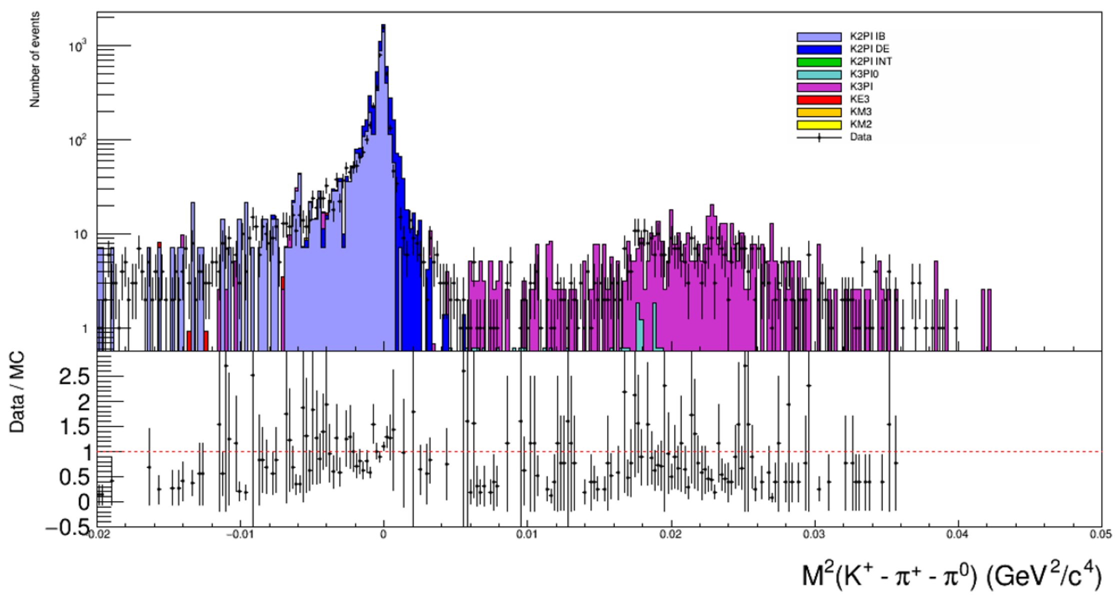

Figure 7: m_{miss}^2 distribution before 2D trapezoidal cut.

A final 2D trapezoidal cut, shown in Fig.4, 5 and 6, defined by:

$$p_T^2 > 6.5 \times 10^{-3}\,\mathrm{GeV}^2/c^2 \quad \mathrm{OR} \quad p_T^2 + 1.03\,m_{\mathrm{miss}}^2 c^2 > 10^{-2}\,\mathrm{GeV}^2/c^2 \tag{6}$$

was applied in [1]. This cut was a compromise between ease of implementation and the minimisation of this quantity:

$$\frac{N_{K_{2\pi a\text{-like}}}^{m_a=0}}{N_{K_{2\pi a\text{-like}}}} \tag{7}$$

with $N_{K_{2\pi a\text{-like}}}$ being the number of events from the $K2\pi$ MC sample and $N_{K_{2\pi a\text{-like}}}^{m_a=0}$ the number of events from the signal MC sample in the massless case passing the signal selection. However, this trapezoidal cut could be improved by using a triangular cut, which would more effectively eliminate the $K2\pi$ (IB) background and perform better for higher axion masses. Additionally, this cut could be slicing, i.e. adapted based on different mass hypotheses. For now, as a first approximation, we have re-implemented the trapezoidal cut.

4.3.4 Normalisation analyzer

On top of preselection the K2PI flag is required. The normalisation analyzer aims, in fact, at selecting the $K_{2\pi}$ decays, chosen as normalisation channels as explained in Sec.4.4. In Fig.8, the $m_{\gamma\gamma}$ distribution after the normalisation selection is shown. The MC samples for the background channels are stacked on one another, while the data are plotted separately. It is possible to see that only the $K2\pi$ events survive this normalisation selection.

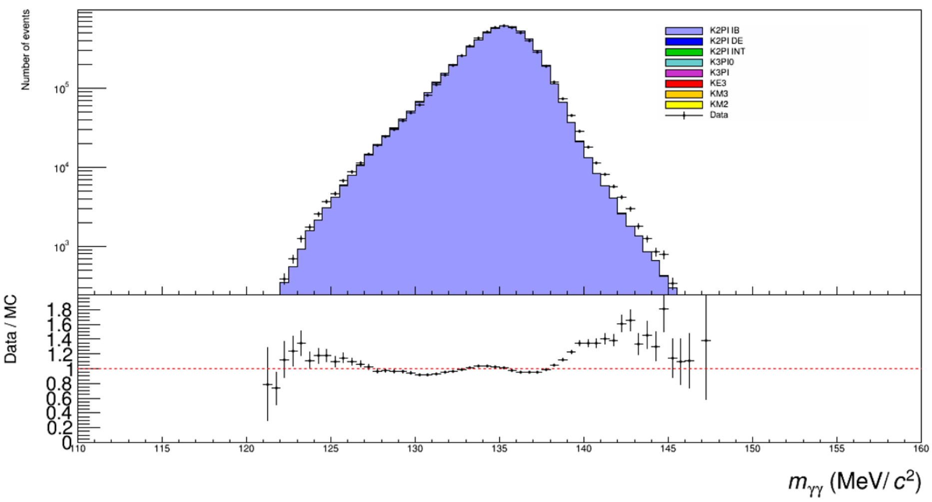

Figure 8: $m_{\gamma\gamma}$ distribution after the normalisation selection.

Note that the "wave effect" observed in the data/MC ratio plot in Fig. 8 is primarily due to the peak effect and some discrepancies between the MC and data resolutions.

4.4 Normalisation Procedure

The number of kaon decays, N_K^{data}, that occurred in the fiducial region during the data-taking period is not known *a priori*. Additionally, a comparison between the sum of all Monte Carlo (MC) contributions and the data must be performed. In order to do this comparison, each MC sample i must be rescaled to match the number of kaon decays observed in the data. After rescaling, the MC contributions can be summed.

To compute the scale factor f^i for each MC sample i, both the number of generated kaons, N_{gen}^i, and the number of kaons in the data, N_K^{data}, must be known.

The number of K mesons generated in each Monte Carlo sample i, N_{gen}^i, is calculated by integrating the histogram of the vertex position z_{vtx} of the MC truth events within the fiducial region (105-180 m). Once N_{gen}^i and the decay branching ratio BR^i are known, the number of kaon decays N_K^i in each sample can be estimated as:

$$N_K^i = \frac{N_{gen}^i}{BR^i} \tag{8}$$

Regarding the direct emission (DE) and interference (INT) terms of the $K^+ \to \pi^+\pi^0\gamma$ decay, the relative contributions of DE and INT with respect to inner Bremsstrahlung (IB) are provided [9] for $T^*_{\pi^+} < 80$ MeV, where $T^*_{\pi^+}$ is the kinetic energy of the charged pion in the kaon rest frame. To ensure the conditions for using the provided relative branching ratios (BR), a cut on the MC truth $T^*_{\pi^+}$ was applied at the beginning of the preselection for the DE and INT samples. This procedure allowed the extraction of the z_{vtx} distribution exclusively for decays where $T^*_{\pi^+} < 80$ MeV. Consequently, N_{gen}^i and $N_K^{\text{DE, INT}}$ can be estimated using the provided relative DE and INT contributions.

An alternative approach involves analyzing the MC truth $T^*_{\pi^+}$ distributions for DE (Fig. 9a) and INT (Fig. 9b) calculating the fraction of π^+ mesons with $T^*_{\pi^+} > 80$ MeV, which accounts for approximately 13% and 30% for the DE and INT samples, respectively. As a first approximation, the BR can be rescaled by accounting for the fraction of π^+ mesons that fall outside the provided kinetic energy range.

For the data, a normalization selection procedure (Sec.4.3.4) is implemented to select the $K_{2\pi}$ decays. In fact, a good way to estimate N_K^{data} is by identifying a background decay channel with a large branching ratio (BR) to minimize the uncertainty in the BR. This channel should mimic the signal so that the normalization selection has very similar efficiency for both the signal and the chosen channel. By selecting the $K_{2\pi}$ decay, we have:

$$N_{K2\pi}^{\text{data}} = N_K^{\text{data}} \cdot BR^{K2\pi} \cdot \varepsilon^{K2\pi} \tag{9}$$

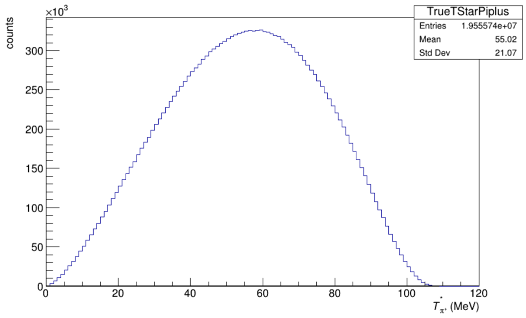

(a) $T^*_{\pi^+}$ distribution DE component.

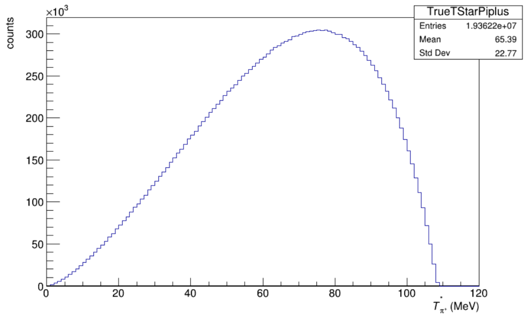

(b) $T^*_{\pi^+}$ distribution INT component.

Figure 9: Comparison of $T^*_{\pi^+}$ distributions for DE and INT components.

where $N^{\text{data}}_{K2\pi}$ is the number of events in the data sample passing the normalization selection, and $\varepsilon^{K2\pi}$ is the normalization selection efficiency. $\varepsilon^{K2\pi}$ can be computed as:

$$\varepsilon^{K2\pi} = \frac{N^{\text{MC}}_{K2\pi,\text{sel}}}{N^{\text{MC}}_{K2\pi,\text{gen}}} \tag{10}$$

where $N^{\text{MC}}_{K2\pi,\text{sel}}$ is the number of events in the $K_{2\pi}$ MC sample passing the normalization selection, and $N^{\text{MC}}_{K2\pi,\text{gen}}$ is the number of $K_{2\pi}$ generated events.

Therefore, starting from Eq.10, the number of kaon decays in the data sample can be estimated as:

$$N^{\text{data}}_{K} = \frac{N^{\text{data}}_{K2\pi}}{BR^{K2\pi} \cdot \varepsilon^{K2\pi}} \tag{11}$$

Since a downscaling factor of D_{K2PI} is applied to the events labeled as K2PI in the data sample, each K2PI event in the data sample is weighted with $w = D_{K2PI}$ when generating the histograms.

Finally, each MC sample is scaled by a factor $f^i = \frac{N^{\text{data}}_K}{N^i_K}$.

5 Conclusions

In this analysis, the cuts from the preliminary sensitivity study were reimplemented and, when possible, improved. A key advancement in this work is the inclusion of the direct emission (DE) and interference (INT) background contributions, which were not accounted for in previous studies. This has enabled a more thorough evaluation of backgrounds that could affect the sensitivity of the search in the case of vanishing mass $m_a = 0$ MeV.

Further investigation is required to more effectively suppress the K3PI background. Additionally, more effort is needed to refine the trapezoidal cut. It would also be valuable to explore the Dalitz plot cut used in the analysis conducted by the OKA collaboration [7] for potential improvements. Expanding the dataset to include all data from the 2017 run will also be crucial for the analysis.

Finally, estimating the 90% upper limit on the branching ratio of the decay $K^+ \to \pi^+\pi^0 a$ using the CLs method remains an essential next step.

References

[1] P. L. Chiatto, A. Bizzeti, and F. Bucci, "First estimate of the sensitivity for the decay $K^+ \to \pi^+\pi^0 a$." NA62 Internal Note NA62-22-01, 2022.

[2] J. Martin Camalich, M. Pospelov, P. Vuong, R. Ziegler, and J. Zupan, "Quark flavor phenomenology of the QCD Axion," *Phys. Rev. D*, vol. 102, no. 1, p. 015023, 2020.

[3] E. Cortina Gil *et al.*, "Search for a feebly interacting particle X in the decay $K^+ \to \pi^+ x$," *JHEP*, vol. 03, p. 058, 2021.

[4] J. M. P. et al., "Revised experimental upper limit on the electric dipole moment of the neutron," *Phys. Rev. D*, vol. 92, p. 092003, 2015.

[5] M. Reece, "TASI Lectures: (No) Global Symmetries to Axion Physics," April 2023. Department of Physics, Harvard University, Cambridge, MA, 02138.

[6] O. Tchikilev *et al.*, "Search for light pseudoscalar sgoldstino in k413 decays," *Phys. Lett. B*, vol. 602, pp. 149–156, 2004.

[7] A. Sadovsky, A. Filin, S. Akimenko, *et al.*, "Searches for the light invisible axion-like particle in $K^+ \to \pi^+\pi^0 a$ decay," *Eur. Phys. J. C*, vol. 84, p. 266, 2024.

[8] E. C. Gil *et al.*, "The beam and detector of the NA62 experiment at CERN," *Journal of Instrumentation*, vol. 12, no. 5, p. P05025, 2017.

[9] J. The NA48/2 Collaboration, Batley, G. Kalmus, *et al.*, "Measurement of the direct emission and interference terms and search for CP violation in the decay $K^\pm \to \pi^\pm\pi^0\gamma$," *Eur. Phys. J. C*, vol. 68, pp. 75–87, 2010.

[10] K. O. et al. (Particle Data Group), "Review of particle physics," *Chin. Phys. C*, vol. 38, p. 090001, 2014.